

# Electrochemical Sensing Platform Based on Functionalized Multi-Walled Carbon Nanotubes and Metal Oxide for the Detection and Degradation Studies of Orange II Dye

Muhammad Irfan, Afzal Shah,\* Faiza Jan Iftikhar, Mazhar Hayat, Muhammad Naeem Ashiq, and Iltaf Shah\*



Cite This: *ACS Omega* 2022, 7, 32302–32312



Read Online

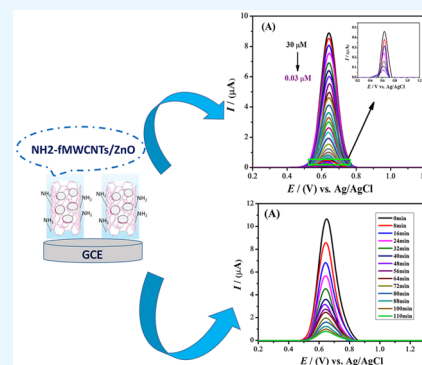
ACCESS |

Metrics & More

Article Recommendations

Supporting Information

**ABSTRACT:** Textile industry effluents are heavily contaminated with dyes. The discharge of these toxic dyes into waterbodies poses a serious threat to aquatic flora and fauna. The ultimate entrance of these toxins from thereon into the food chain affects the primary and secondary consumers. Therefore, the adoption of a sustainable solution for protection against the detrimental effects associated with adulterated water is an immediate need of the hour. To address the severity of the issue, the present work aims to design an electrochemical sensing platform by modifying the glassy carbon electrode (GCE) with zinc oxide nanoparticles and amino group-functionalized multi-walled carbon nanotubes (NH<sub>2</sub>-fMWCNTs) for the detection of Orange II, which is a toxic azo dye. Zinc oxide nanoparticles facilitate electron transfer between the transducer and the analyte. While, the positively charged NH<sub>2</sub>-fMWCNTs in acidic medium help in preconcentration of negatively charged analyte molecules at the electrode/electrolyte interface. The modification of the GCE catalyzed the oxidation of Orange II, as evidenced by the negative shift of the oxidation potential and enhancement in peak current intensity. Square wave voltammetry was used to optimize various experimental conditions, such as the supporting electrolyte, pH of the electrolyte, deposition potential, and deposition time for the best performance of the designed sensor. Under the optimized conditions, the detection limit and quantification of the designed sensor were found to be 0.57 and 1.92 nM, respectively. The catalytic degradation studies of Orange II was shown to be facilitated by titanium dioxide, which acted as a photocatalyst. The addition of hydrogen peroxide further promoted the extent and rate of degradation of dye. The breakdown of Orange II was probed by the designed sensing platform electrochemically and also by UV–visible spectroscopy. The dye degraded up to 92% by following pseudo-first-order kinetics.



## 1. INTRODUCTION

Due to continuous rise in human population, the world is confronting complex problems related to health, food, energy, scarcity, and environmental pollution. In recent decades, energy crisis and environmental pollution have captured the attention of the whole world.<sup>1</sup> Several research groups are working to address the root issues that have contributed to the rapid increase in environmental pollution and its associated health risks.<sup>2</sup> One of its main causes is the rapid increase in population and the consequent surge in maintaining a good standard of living.<sup>3</sup> Fulfillment of these needs has led to large-scale industrialization. Additionally, the use of chemicals has increased with the growth of modern industries, leading to an enhanced contribution to environmental pollution.<sup>4</sup> These chemicals are responsible for the destruction of marine life, severe health diseases like immune suppression, asthma, stroke, tumor, hepatitis, cancer, respiratory failures, chronic illness, and many more.<sup>5</sup>

Today, one of the biggest issues is water contamination. To this end, synthetic dyes are the major contributor to water pollution due to their large production and usage throughout

the world. The textile industry has been the biggest consumer of water among all industries and at the same time is responsible to release harmful wastes into water bodies. These toxic dyes impart serious threats to the stability of the environment.<sup>6</sup> These are carcinogenic and mutagenic, causing a number of diseases. However, among all synthetic dyes, azo dyes are more toxic to human and aquatic life.<sup>7</sup>

Orange II dye belongs to the family of azo dyes that are abundantly expended in the textile and wool industry. Although this dye has been proven to be seriously dangerous for health causing lowering of red blood cells and reducing cell volume,<sup>8</sup> it can still be found in trace amounts in certain foods such as sauces and chilli.<sup>9</sup> Moreover, though the dye is banned

**Received:** June 11, 2022

**Accepted:** August 23, 2022

**Published:** September 2, 2022



in China, even then it is being used to preserve foodstuff.<sup>10</sup> Azo dyes are also used as coloring agents in cosmetics and pharmaceutical industries.<sup>11</sup> Different methods are being used to remove this toxic dye from water.<sup>12</sup> However, the need of the hour is to develop vigorous, inexpensive, and green techniques for the elimination of this hazardous dye.<sup>13</sup>

Various methodologies have been employed to detect and remove the toxic dye Orange (II) from water samples.<sup>10</sup> Recently, techniques like spectroscopy and polarography have been used for the analysis of Orange II.<sup>14</sup> These techniques are somehow limited and unsuitable for *in situ* study, due to their complex instrumentation, less sensitivity, and longer analysis time. As a result, these methods can be replaced by a cost-effective voltammetric method for easy handling and quick analysis of the samples.<sup>15</sup> Sensors are the best option for analyte analysis, owing to their appropriate size, excellent sensitivity, specificity, prompt response, and cost-effectiveness.<sup>16</sup>

So far, different kinds of materials have been used for the development of sensors. Among them, functionalized multi-walled carbon nanotubes and zinc oxide (ZnO) nanoparticles have demonstrated appealing properties for detecting target molecules. In this regard, ZnO nanomaterials have garnered much attention due to their numerous properties and outstanding characteristics.<sup>17</sup> ZnO has high binding energy, high surface area, and biological compatibility.<sup>18</sup> The sensors built upon these nanomaterials show instant response to toxic chemicals due to the small granular size of nanoparticles.<sup>19</sup> Hence, ZnO-based sensors show a variety of applications due to their porous structures.<sup>20</sup>

Carbon nanotubes (CNTs) are used in the preparation of sensors due to their enhanced qualities. They possess high electrical, mechanical, and thermal characteristics.<sup>21</sup> CNT-based sensors are considered one of the most attractive topics for researchers worldwide. Amino functionalization has been the most promising and interesting kind of modification of CNTs. The amino ( $-\text{NH}_2$ ) group's electron-donating and nucleophilicity properties result in activation of the surface of CNTs for a variety of applications. Thus, the amino group-functionalized multi-walled carbon nanotubes ( $\text{NH}_2$ -fMWCNTs) have demonstrated high sensitivity, excellent selectivity, and good stability toward a wide range of analytes.<sup>22</sup> Here in this work, ZnO nanoparticles have been used as a catalyst to enhance the electrochemical signals of glassy carbon electrode (GCE) and hence improve the performance of the modified electrode surface [ $\text{NH}_2$ -fMWCNTs/ZnO/GCE].

In recent years, contaminated drained effluents in water bodies have increased with a boom in industrialization, which has posed a serious problem for removing these toxic chemicals in a robust manner. To meet this need, scientists have developed methods to degrade and mineralize organic contaminants by leveraging photocatalysis. Photocatalysis is a promising approach in comparison to conventional catalytic methods studied till date.<sup>23</sup> Photocatalysts are semiconductor-based nanostructures that have gained importance as they are cost-effective.<sup>24</sup> According to the band gap theory, semiconductor materials, on exposure to light, are capable to conduct electricity even at room temperature, hence behave as photocatalysts. This photoexcitation state upon solar irradiation causes the generation of electron-hole pairs ( $e^-h^+$ ).  $\text{TiO}_2$  is the best and most environmentally safe nanoparticle. Titania shows excellent photocatalytic features such as high efficiency, cost-effectiveness, photostability, being environ-

mentally friendly, and so on.<sup>25</sup> To enhance the activity of  $\text{TiO}_2$  nanoparticles, hydrogen peroxide has been used in the photodegradation methodology. It not only behaves as an electron acceptor to avoid the recombination but also causes the generation of  $\bullet\text{OH}$  and  $\bullet\text{O}_2$  (reactive oxygen species) on the catalyst's surface. The intense oxidative ability of both  $\bullet\text{OH}$  and  $\bullet\text{O}_2$  is helpful to degrade organic dyes in water.<sup>26</sup> Therefore, to enhance the degradation rate,  $\text{TiO}_2$  nanoparticles and  $\text{H}_2\text{O}_2$  were used for Orange II dye degradation. In the present research work, Orange II dye was electrochemically detected at the designed sensor made up of GCE modified with ZnO nanoparticles and  $\text{NH}_2$ -fMWCNTs. Moreover, the dye was removed from water samples using  $\text{H}_2\text{O}_2$  and  $\text{TiO}_2$  nanoparticles.

## 2. EXPERIMENTAL SECTION

**2.1. Reagents and Materials.** All the chemicals used in the experimental section were of analytical grade. The pristine functionalized multi-walled carbon nanotubes ( $\text{NH}_2$ -fMWCNTs), zinc oxide (ZnO), and  $\text{TiO}_2$  nanoparticles were purchased from Merck Pte. Ltd. Singapore and used in preparation of the sensor. All other chemicals including Orange II dye were obtained from Sigma-Aldrich Chemie GmbH, Germany. To prepare the stock solutions, doubly distilled water was used. The phosphate buffer solution (PBS), Britton Robinson buffer (BRB), and solutions of  $\text{H}_2\text{SO}_4$ , HCl, NaOH, KCl, and NaOH were used for studying the effect of various supporting electrolytes. For the investigation of the interference effect, the organic compounds [Nile blue sulphate (NBS), Malachite green (MG), Rhodamine B (RB), and ethyl violet (EV)] and metal salts (potassium phosphate, calcium bicarbonate, cobalt chloride, sodium carbonate, and zinc chloride) were used.

**2.2. Instrumentation.** Impedimetric and voltammetric measurements for ensuring successful electrode fabrication and sensor development were carried out *via* Multichannel Metrohm Autolab (Utrecht, The Netherlands) M101, PGSTAT302N, FRA32M, F120-Integrator running with electrochemical software frequency resonance analyzer, general purpose electrochemical system, and NOVA 1.11 software, respectively. The electrochemical cell consisted of a doubly walled glass cell having a cell top model K64 PARC. The cell top comprised an easily replaceable self-mounting plastic cap having five standard taper ports; three for insertion of electrodes (auxiliary electrode, working electrode, and reference electrode), while two served as the inlet and outlet for inert gas purging. Additionally, the cell was also linked to the thermostat model LAUDA K-4R (USA) through a side opening to maintain the temperature throughout the measurements. For the study of photodegradation of Orange II dye, a Shimadzu UV-1700 spectrophotometer (Japan) was used. The absorption spectra of the material were recorded in the wavelength range of 200–800 nm.

**2.3. Electrode Modification and Detection Procedure.** The stock solution of the analyte was prepared with a concentration of 0.1 mM in distilled water. For electrochemical investigations, stock solution was then diluted to 30  $\mu\text{M}$  by using the same solvent. To prepare the modifier solutions of concentration 1 mg/mL of each  $\text{NH}_2$ -functionalized MWCNTs and ZnO NPs, the mixture was ultrasonicated for 1 h in the presence of DMF. To conduct the electrochemical analysis of the analyte, it was ensured that before each scan, polishing of a bare glassy electrode was carried out to give it a

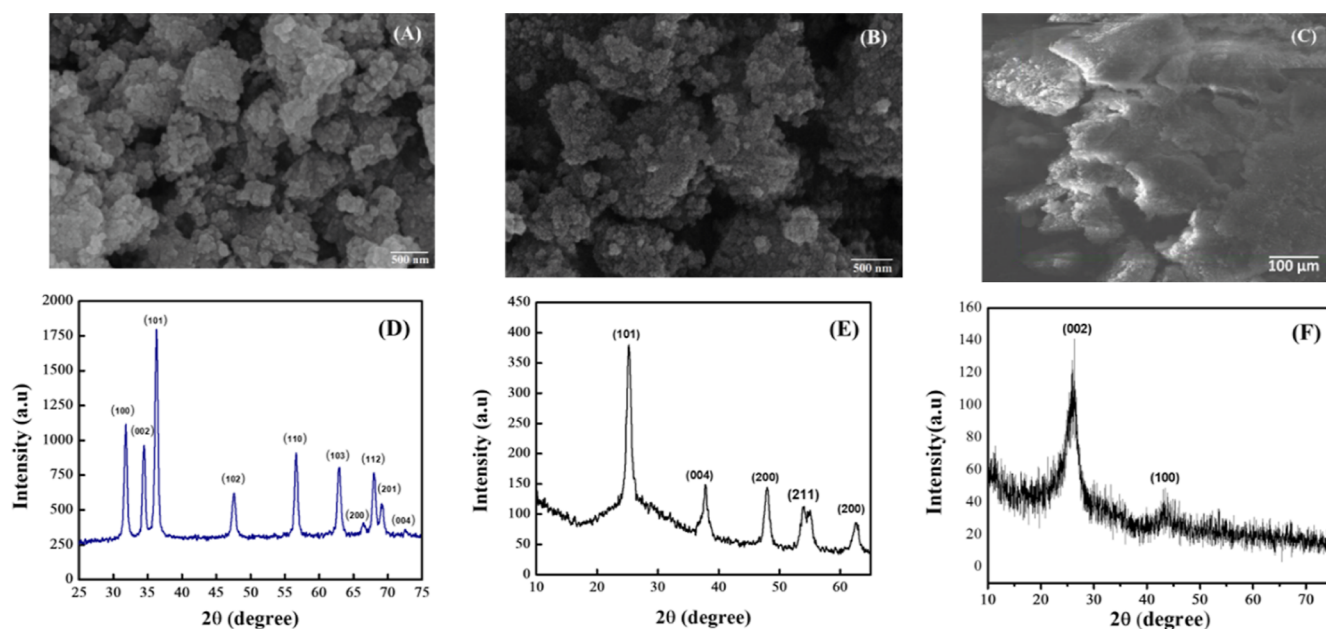


**Figure 1.** Structural characterization: (A) SEM image of ZnO nanoparticles. (B) SEM image of TiO<sub>2</sub> nanoparticles. (C) SEM image of NH<sub>2</sub>-fMWCNTs. (D) XRD pattern of ZnO nanoparticles. (E) XRD pattern of TiO<sub>2</sub> nanoparticles. (F) XRD pattern of NH<sub>2</sub>-fMWCNTs.

clear mirror-like surface. For the polishing of the electrode, a drop of water was placed on a nylon buffing pad before each measurement.

This buffing pad contained alumina powder with the particle size of 1  $\mu\text{m}$ .<sup>27</sup> The electrode surface was rubbed in a manner of digit eight, resulting in smooth appearance, on the buffing pad. The ultimate goal of rubbing was to avoid the presence of grooves on the surface of the electrode. The rubbing of the electrodes was followed by rinsing using a jet of distilled water to remove all the impurities and unwanted particles.<sup>28</sup> After ensuring that the electrode's surface was free from impurities, cyclic voltammograms were recorded by placing the GCE in the supporting electrolyte until a constant baseline voltammogram was obtained.<sup>29</sup> After ensuring that GCE was free from impurities, it was modified by using layer by layer drop-casting of 5  $\mu\text{L}$  of ZnO NPs and 5  $\mu\text{L}$  of NH<sub>2</sub>-functionalized MWCNTs, which was then left for air drying. Once dried, a 10  $\mu\text{L}$  drop of analyte solution was cast on the pre-modified surface of the GCE.<sup>30</sup> It was then placed in PBS, and a pulse voltammograms of the analyte were recorded. Electrochemical impedance spectroscopy (EIS) was employed for studying the behavior of the modified electrode. Compound analysis was carried out using a variety of techniques, including square wave voltammetry (SWV) and cyclic voltammetry (CV). SWV analysis was conducted for quantification purpose and detection limit.

UV-visible spectrophotometry was carried out along with SWV for studying the degradation process. The solution of the analyte was kept under direct sunlight. A known amount of the photocatalyst was added, followed by addition of H<sub>2</sub>O<sub>2</sub> to speed up the degradation process. Samples were taken out at different time intervals, and corresponding voltammograms and spectra were recorded. The percentage degradation was calculated by using the data obtained by both techniques.

### 3. RESULTS AND DISCUSSION

**3.1. Material Characterization.** Scanning electron microscopy (SEM) and X-ray diffraction (XRD) were

employed to reveal information about the morphology of ZnO, TiO<sub>2</sub> nanoparticles, and NH<sub>2</sub>-fMWCNTs. Figure 1A shows the SEM micrograph of the ZnO nanoparticles at a magnification of 100,000 $\times$ , suggesting that the particles were agglomerated and had an irregular spherical morphology. Agglomeration might have taken place due to the polarity and electrostatic attraction existing between the ZnO nanoparticles. The TiO<sub>2</sub> nanoparticles were slightly agglomerated and exhibited an approximate spherical morphology as evident from the SEM micrograph, as shown in Figure 1B. The SEM micrograph of NH<sub>2</sub>-fMWCNTs is shown in Figure 1C, and it can be inferred from the SEM image that the nanoporous structure of NH<sub>2</sub>-fMWCNTs would remarkably increase the surface area of GCE. The X-ray diffractogram of ZnO nanoparticles, as shown in Figure 1D, consisted of peaks positioned at angles of 31.8, 34.5, 36.2, 47.5, 56.6, 62.8, 66.5, 68, 69.2, and 72.6 $^\circ$  corresponding to (100), (002), (101), (102), (110), (103), (200), (112), (201), and (004) diffraction planes, respectively. The XRD studies revealed that the ZnO nanoparticles had a hexagonal wurtzite structure according to JCPDS number 36-1451. The XRD pattern of TiO<sub>2</sub>, as shown in Figure 1E, consisted of peaks positioned at angles of 25.05, 37.8, 48.02, 54.8, and 62.6 $^\circ$  corresponding to (101), (004), (200), (211), and (200) crystal planes, respectively. In the light of the JCPDS number 00-001-0562 for TiO<sub>2</sub>, it has a tetragonal structure. The average crystallite size of ZnO and TiO<sub>2</sub> nanoparticles was determined using the Debye-Scherrer formula and was found to be 48 and 9.67 nm, respectively. XRD analysis was employed to investigate the crystallinity of the NH<sub>2</sub>-fMWCNTs. Figure 1F shows diffraction peaks positioned at 26.1834 and 43.22 $^\circ$  corresponding to (002) and (100) diffraction planes, respectively, which are indexed to the hexagonal graphite peak for the carbon nanotubes (JCPDS no. 41-1487). The diffraction peaks of NH<sub>2</sub>-fMWCNTs were broad and exhibited low intensity, owing to the disruptions in the pristine structure.

**3.2. Electrochemical Characterization.** A significant factor influencing the performance of the electrochemical

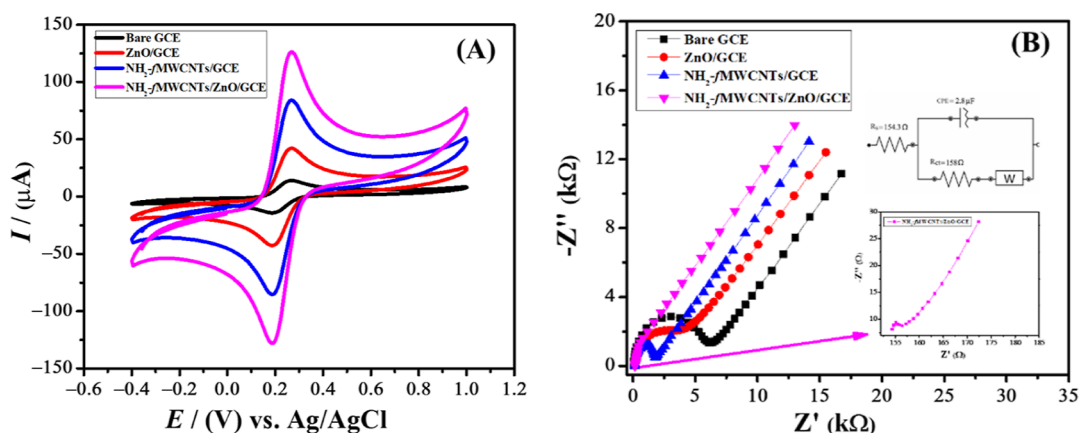


**Figure 2.** (A) Cyclic voltammograms of bare and modified GCE in 5 mM  $K_3[Fe(CN)_6]$  with 0.1 M KCl as a supporting electrolyte at a scan rate 100  $mV s^{-1}$ . (B) Nyquist plots of bare and modified GCE in a solution of 5 mM  $K_3[Fe(CN)_6]$  as a redox probe and 0.1 M KCl as a supporting electrolyte.

sensing platform is the area of the working electrode surface. The cyclic voltammetric experiment was carried out for the investigation of the electroactive surface area of the electrodes by using 5 mM  $K_3Fe(CN)_6$  as a redox probe at room temperature by using 0.1 M KCl as the electrolyte. The current response of  $[Fe(CN)_6]^{3-/4-}$  at bare, ZnO, NH<sub>2</sub>-fMWCNTs, and NH<sub>2</sub>-fMWCNTs/ZnO modified GCE was investigated. The Randles–Sevcik equation ( $I_p = 2.69 \times 10^5 n^{3/2} AD^{1/2} \nu^{1/2} C$ ) was used to calculate the electroactive surface area of bare and modified electrodes, respectively.<sup>31</sup> Here,  $I_p$  represents the anodic peak current in Amperes,  $D$  is the analyte's diffusion coefficient in  $cm^2 s^{-1}$ ,  $n$  the number of electrons,  $A$  is the electroactive surface area in  $cm^2$ ,  $\nu$  is the scan rate with potentials being swept across the electrode in units of  $V s^{-1}$ , and  $C$  is the concentration of the probing analyte in  $mol cm^{-3}$ . For  $K_3Fe(CN)_6$ ,  $D = 7.6 \times 10^{-6} cm^2 s^{-1}$ , and  $n = 1$ . Electroactive surface areas for GCE, ZnO/GCE, NH<sub>2</sub>-fMWCNTs/GCE, and NH<sub>2</sub>-fMWCNTs/ZnO/GCE are shown in Table S1. The active surface area of NH<sub>2</sub>-fMWCNTs/ZnO/GCE increased almost six times than the active surface area of the bare electrode. An enhancement in peak current can be noticed in Figure 2A. There are more binding sites on the surface of the electrode for analyte molecules to cling because of the presence of NH<sub>2</sub>-fMWCNTs/ZnO.

Through EIS, the charge transferability of both bare and modified GCEs was investigated. A solution of 5 mM  $K_3[Fe(CN)_6]$  was used as a redox probe and 0.1M KCl solution as a supporting electrolyte. At 10 mV amplitude, a frequency range of 100 kHz to 0.1 Hz was applied. Nyquist plots using data obtained at bare GCE, ZnO/GCE, NH<sub>2</sub>-fMWCNTs/GCE, and NH<sub>2</sub>-fMWCNTs/ZnO/GCE are illustrated in Figure 2B. The semicircle portion of the Nyquist plot represents the charge-transfer resistance ( $R_{ct}$ ), whereas the linear portion of the plot at lower frequencies represents diffusional limited processes (Warburg impedance). The Warburg element ( $Z_w$ ) has been added in the Nyquist plot as a standard electrochemical interface. This element represents resistance due to translational motion (also known as diffusion) of the mobile oxidized and reduced species of the redox probe (here 5 mM  $K_3[Fe(CN)_6]$ ) in the depletion layer caused by a changing excitation signal. This improvement in charge-transfer resistance is related to the electrochemical reaction that adds a distinctive line at 45° to the Nyquist plot

at low frequencies. Charge-transfer resistance can be determined by the diameter of the semicircle at a higher frequency.<sup>32</sup> The  $R_{ct}$  value greatly decreased after the modification of GCE with NH<sub>2</sub>-fMWCNTs/ZnO, as shown in inset Figure 2B. Hence, the surface area of the modified electrode increased as a result of provision of more active sites for the analyte. Adsorbed molecules on the surface of GCE act as a bridge between Orange II and the electrode. In this way, electron transfer becomes faster after the modification of the electrode. The inset in Figure 2B shows an equivalent circuit model with a resistor, capacitor, Warburg impedance, and constant phase element that was fitted to the experimental data. Due to the difference in impedance parameters between the modified and unmodified GCE, it can be concluded that the transducer used in this investigation was successfully fabricated. It can be seen from Table S2 that the charge-transfer resistance of NH<sub>2</sub>-fMWCNTs/ZnO/GCE is lower among all other modified and bare electrodes. Reduction of the interfacial barrier is responsible for the rapid charge-transfer rate on the surface of the modified electrode. The lowest value of charge-transfer resistance for the GCE modified with NH<sub>2</sub>-fMWCNTs/ZnO/GCE reveals faster electron transferability.

**3.3. Voltammetric Analysis of the Target Analyte.** The peak current response of the Orange II at bare and modified electrodes was investigated in PBS of pH 6.0 by SWV. Voltammograms of 30  $\mu$ M concentration of Orange II were recorded at bare and modified electrodes in a potential window of 0.2–1.2 V, as illustrated in Figure 3. The combination of NH<sub>2</sub>-fMWCNTs/ZnO/GCE exhibits the highest current response when compared to the bare GCE, ZnO/GCE, and NH<sub>2</sub>-fMWCNTs/GCE. The electron transfer between the transducer and the analyte was stepped up by employing ZnO.<sup>33</sup> The synergistic effects of the components of the modified sensing platform (NH<sub>2</sub>-fMWCNTs/ZnO/GCE) boosted the oxidation current of the dye by providing greater surface area. Therefore, the intensity of the signal of the analyte was increased to about three folds after modification. Here, ZnO nanoparticles play the role of the mediator between GCE and dye molecules, leading to enhanced electrochemical oxidation signals. ZnO acts like a stepping stone for the transfer of electrons from the dye to the GCE via the NH<sub>2</sub>-fMWCNTs through a hopping mechanism, which offers faster electrochemicals than the tunnelling mechanism, as reported in the literature.<sup>34</sup> The immobilization of ZnO onto the NH<sub>2</sub>-

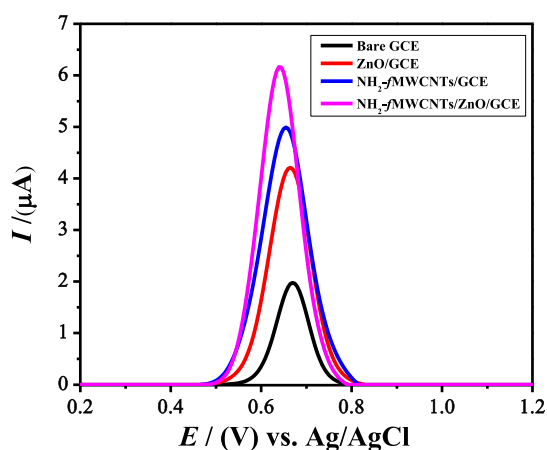


**Figure 3.** SWVs of 30  $\mu\text{M}$  Orange II on bare, ZnO/GCE,  $\text{NH}_2$ -fMWCNTs/GCE, and  $\text{NH}_2$ -fMWCNTs/ZnO/GCE in the supporting electrolyte of PBS (pH 6.0) at a scan rate of 100  $\text{mV s}^{-1}$ .

fMWCNTs leads to an increase in active area of the electrode that facilitates the redox reaction of the dye molecules. Furthermore, the  $\text{NH}_2$ -fMWCNTs/ZnO/GCE has lower  $R_{ct}$  as compared to other combination of modifiers on the GCE, which confirms that surface is facilitating the transfer of electron.

The positively charged  $\text{NH}_2$ -fMWCNTs had a greater affinity for the negatively charged analyte in the acidic medium. The oxidation potential of the analyte at bare GCE was observed at 0.67 V and after the modification of GCE with  $\text{NH}_2$ -fMWCNTs/ZnO, it was shifted toward less potential (0.64 V). This depicts that the modifier helps in the accumulation of the analyte by enhancing the surface area of the electrode.

**3.4. Effect of Scan Rates.** Cyclic voltammograms were obtained to investigate the effect of different scan rates on the anodic peak current of the analyte. Various scan rates ranging from 25 to 150  $\text{mV s}^{-1}$  were studied to confirm whether the reaction of the analyte is surface-controlled or diffusion-controlled.<sup>35</sup> The intensity of peak current increased linearly with the scan rate, as illustrated in Figure S1A. According to literature survey, it has been concluded that if the plot between the log of oxidation peak current and log of the scan rate gives a slope value equals to 0.5, then this process should be

controlled by diffusion. However, the process should be adsorption controlled if the slope value equals to 1.<sup>36</sup> Figure S1B depicts that the slope value is equal to 0.83, which suggests that both processes were involved. The straight line equation is shown in Figure S1B. Since the correlation coefficient in the plot of oxidation peak current versus scan rate is higher (Figure S1C) than the  $R^2$  between peak current versus the square root of the scan rate (Figure S1D), the adsorption process is more favorable on the surface of the electrode. Therefore, the diffusion-controlled process is less pronounced as compared to the surface-assisted process.

**3.5. Optimization of Experimental Parameters.** One of the most sensitive and fast pulse techniques is the SWV. The detection limits of this technique can be compared to those of chromatographic and spectroscopic techniques. The SWV method was used to optimize several experimental parameters to achieve the maximum peak current after the sensing capacity of the modified GCE was verified using a variety of methods, including EIS, CV, and SWV.

**3.5.1. Influence of the Supporting Electrolyte, pH of the Electrolyte, Volume of Modifiers Used, Deposition Potential, and Deposition Time.** The supporting electrolyte is an important analytical parameter for obtaining a well-resolved voltammogram. The shape, position (potential), and intensity of the peak are all influenced by the supporting electrolyte. For the purpose, the analyte (Orange II dye) was tested in a variety of supporting electrolytes, that is,  $\text{H}_2\text{SO}_4$ , HCl, NaOH, KCl, NaOH, BRB (pH = 6.0), and PBS (pH = 6.0). The most appropriate supporting electrolyte was PBS, which provided the best current response and a well-defined peak shape when compared to other electrolytes. As shown in Figure S2A,B, the designed sensor ( $\text{NH}_2$ -fMWCNTs/ZnO/GCE) provided the highest current response in PBS for the analyte. Thus, PBS was chosen as the supporting electrolyte for further investigation.

The pH of the supporting electrolyte also influences the peak potential and peak current. The effect of pH on current response of Orange II dye was studied in PBS as the electrolyte with pH values ranging from 3 to 12. The maximum value of  $I_p$  was found in PBS of pH 6.0, as illustrated in Figure 4A. The peak potential was shifted toward lower values with an increase in pH of the electrolyte. The shifting of peak potential indicates proton involvement in the electron-transfer reaction. Based on the calibration plot, the number of electrons and

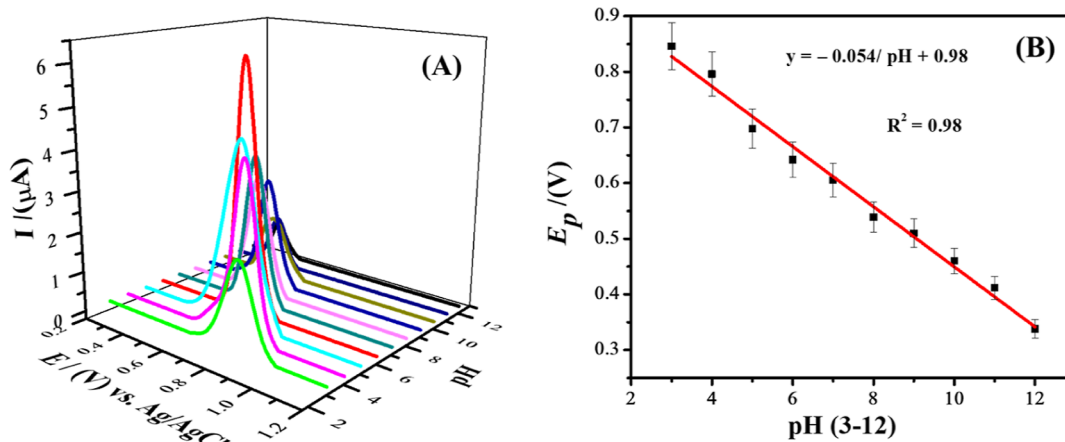


**Figure 4.** (A) SWVs of Orange II analyte in the solution of PBS (pH 3–12) by using  $\text{NH}_2$ -fMWCNTs/ZnO/GCE as a modifier at a scan rate of 100  $\text{mV s}^{-1}$ . (B) Plot of  $E_p$  vs pH of Orange II using PBS as a supporting electrolyte.

## Scheme 1. Proposed Electrochemical Oxidation Mechanism of Orange II at fMWCNTs/ZnO/GCEs

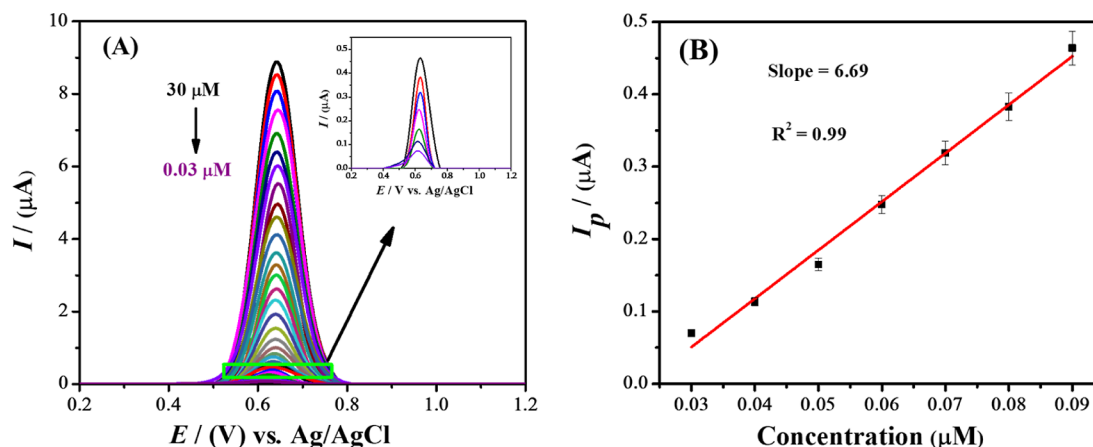
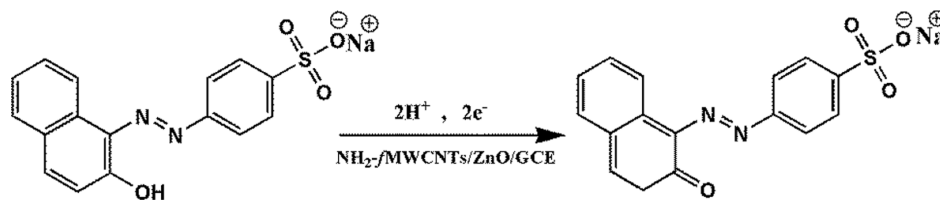


**Figure 5.** (A) Square wave voltammograms of various concentrations of Orange II under pre-optimized conditions at a scan rate of  $100 \text{ mV s}^{-1}$ . (B) Calibration plot obtained by SWV data of lower concentrations under optimized conditions.

**Table 1. Comparison of the Analytical Performance of Different Designed Sensors for the Detection of Orange II Dye**

sr. no	modifying material	$R^2$	method	pH value and supporting electrolyte	LOD (nM)	reference
1	GN-TiO <sub>2</sub> /GCE	0.998	SWV	4.4, HAc-NaAc buffer	0.92	8
2	Cbz-AgNPs/GCE	0.994	SWV	7, BRB buffer	1.2	38
3	PSS-GR/GCE	0.999	LSV	7, PBS	10	39
5	Fe <sub>2</sub> O <sub>3</sub> /MWCNTs-COOH/OP/CPE	0.997	DPV	7, PBS	100	40
6	UiO-66(NH <sub>2</sub> )@Au	0.991	SERS	—	155.86	41
7	NH <sub>2</sub> -MIL-101(Cr)	0.982	SERS	—	142.73	42
8	NH <sub>2</sub> -fMWCNTs/ZnO/GCE	0.998	SWV	6, PBS	0.57	this work

protons involved in the redox process were calculated using the equation:  $\Delta E_p/\Delta \text{pH} = 2.303 mRT/nF$ , where  $R$  is the general gas constant,  $T$  is the temperature,  $F$  is the Faraday constant, and  $m/n$  is the ratio of proton and electron. The slope value calculated from the linear calibration plot is  $54 \text{ mV/pH}$ , as shown in Figure 4B. This value of the slope is nearly close to the Nernstian theoretical value ( $58.5 \text{ mV/pH}$ ), indicating that an equal number of protons and electrons are involved in the oxidation reaction of the analyte (Orange II). Therefore, the proposed oxidation mechanism has been presented in Scheme 1.

The impact of deposition potential ranging from  $-0.1$  to  $0.6 \text{ V}$  was analyzed in PBS of pH 6.0. The peak current of the analyte was enhanced with the increment of deposition potential up to  $0.2 \text{ V}$ , as shown in Figure S3A. Numerous active sites on the surface of the modified electrode were available to the targeted analyte at  $0.2 \text{ V}$ . The peak current decreased as the potential increased due to active sites' saturation. Therefore, the  $0.2 \text{ V}$  deposition potential was selected for further investigations of the Orange II dye (Figure S3B). The optimized potential can assist to achieve excellent sensitivity and high reproducibility of the designed sensor.

Deposition time has a great impact on the electrochemical performance of a modified electrode. For this purpose, the

response of the analyte was recorded by varying deposition time from 5 to 30 s under pre-optimized parameters with the help of SWV. The intensity of peak current goes on increasing with an increase in deposition time as more and more active sites are available on the surface of the electrode. At saturation point, when the analyte gets oriented to all the available active sites, maximum peak current is observed. For maximum response, analyte molecules must be oriented in the proper direction. It has been observed that the Orange II dye showed maximum current intensity at an accumulation time of 20 s (Figure S4B) and after that a decline in the peak current can be observed (Figure S4A).

**3.6. Analytical Applications of the Designed Sensing Platform.** SWV was carried out to investigate the limit of detection (LOD) of the targeted analyte (Orange II dye) under optimized conditions that is,  $0.1 \text{ M}$  PBS of pH 6.0,  $0.2 \text{ V}$  deposition potential, and 20 s deposition time. Figure 5A depicts that the peak current is dependent on the concentration of the analyte. Using SWV, different concentrations of the analyte solution were investigated for detecting the lowest limit at the designed sensor. The inset in Figure 5A shows the current response of the analyte at lower concentrations. A linear calibration curve was obtained by varying the concentration of the analyte from  $0.03$  to  $0.09 \mu\text{M}$ ,

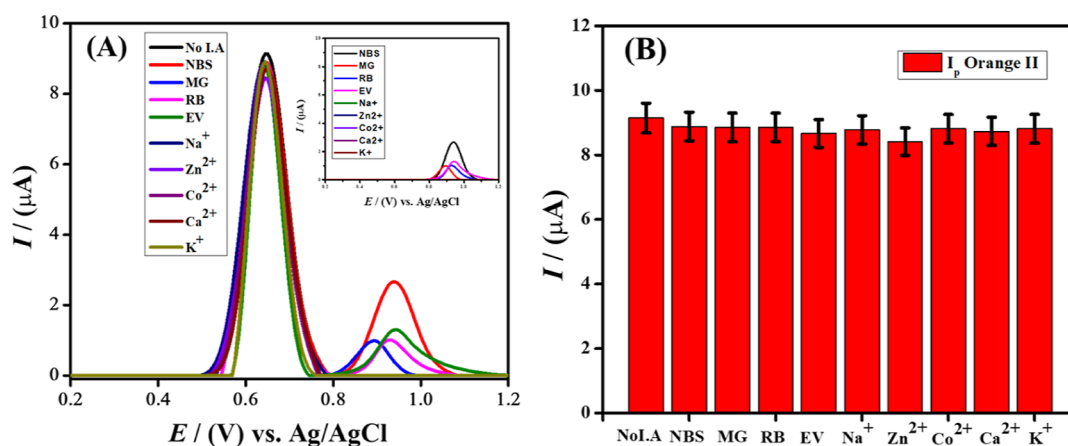


**Figure 6.** (A) Square wave voltammograms of 30  $\mu\text{M}$  Orange II in the presence of different interfering agents. The inset graph with individual interferents in the total absence of Orange II is also presented using 0.1 M PBS of pH 6.0. (B) Bar graph of the peak current of Orange II at the designed sensor ( $\text{NH}_2\text{-fMWCNTs/ZnO/GCE}$ ).

**Table 2. Real Sample Analysis of the Orange II at the Designed Sensor under Optimized Conditions**

dye	sample	initial amount ( $\mu\text{M}$ )	spiked amount ( $\mu\text{M}$ )	found ( $n = 4$ ) ( $\mu\text{M}$ )	RSD (%)	recovery (%)
Orange II	industrial wastewater sample 1	0.0	30	29.5	2.2	98.3
	industrial wastewater sample 2	0.0	30	28.95	2.3	96.5
	fruit juice sample 1	0.0	30	28.80	2.8	96.0
	fruit juice sample 2	0.002	30	29.40 expected (30.001)	3.1	98.0
	ketchup sauce sample 1	0.004	30	28.91 expected (30.005)	3.4	96.4
	ketchup sauce sample 2	0.0	30	28.93	3.2	96.4

as shown in Figure 5B. The detection and quantification limits were calculated by IUPAC guidelines, that is,  $3\sigma/m$  and  $10\sigma/m$ , respectively,<sup>37</sup> where  $m$  represents the slope of the peak current versus concentration plot, and  $\sigma$  denotes the standard deviation of the blank solution. The current values of the blank solution at the peak position were used to calculate the standard deviation. The LOD and limit of quantification at the designed sensor ( $\text{NH}_2\text{-fMWCNTs/ZnO/GCE}$ ) were found to be 0.57 and 1.9 nM, respectively. Table 1 shows the comparison of the designed sensor with the previously reported sensors.

**3.7. Evaluation of the Stability of the Designed Sensor.** The stability of the designed sensing platform was evaluated in terms of its repeatability and reproducibility. The electrochemical response of the proposed sensor in the presence of Orange II dye under pre-optimized experimental conditions served as a measure for determining the sensor's stability. For determining the stability, the  $\text{NH}_2\text{-fMWCNTs/ZnO/GCE}$  was placed in PBS of pH 6.0 for varying time intervals and then subjected to SWV analysis. In comparison to the intensity of the signal of the newly modified electrode, there were no prominent changes observed in the intensity of peak current up to 48 h, as shown in Figure 5SA. The observations suggested that the sensing platform exhibited intra-day and inter-day stability. The designed sensor displayed stability through different time intervals due to poor solubility of the electrode modifier in water, which not only prevented the leaching of the modifier from the electrode surface but also facilitated the retention of the intensity of the peak current of the analyte with time. To ensure that the sensing ability of the designed sensor was reliable, six independent  $\text{NH}_2\text{-fMWCNTs/ZnO/GCEs}$  were fabricated and subjected to SWV analysis. There was no considerable deviation in the current response exhibited in terms of the oxidation peak, as

illustrated in Figure 5SB. The observations suggested that the designed electrochemical sensor had excellent repeatability and remarkable reproducibility. Thus, the designed sensing platform is a dependable sensor for the detection of Orange II dye.

**3.8. Study of Effects of Interferents for Validation of the Designed Sensor.** A real sample collected from some wastewater disposal site near a textile industry may contain additional species other than the analyte. There exists a possibility that these species might be capable of affecting the sensing efficiency of the designed sensor. To find out the effect of interferents on the anodic peak response of the sensing platform, the experimental conditions were replicated by introducing 1 mM of different dyes and metal ions (simulating industrial wastewater) separately as interferents in the 30  $\mu\text{M}$  analyte solution and voltammograms were recorded, as shown in Figure 6A, with the same optimized conditions used as previously. The interferents include different dyes such as NBS, MG, RB, and EV along with metal ions such as  $\text{Na}^+$ ,  $\text{Zn}^{2+}$ ,  $\text{Co}^{2+}$ ,  $\text{Ca}^{2+}$ , and  $\text{K}^+$ . The stability of the fabricated sensor in the presence of different interfering agents is shown in Figure 6B.

**3.9. Application of the Sensor in Real Samples.** The real practices were performed to check the precision and accuracy of the designed sensor. For this purpose, to measure the amount of Orange II dye in industrial wastewater, fruit juice and ketchup sauce were used for real sample analysis. 2 mL of fruit juices and ketchup sauce were diluted to 10 mL by using distilled water. Initially, no contents of Orange II molecules were found in the real matrixes. Then, a known amount of the targeted analyte was spiked by the standard addition protocol. The recovered amount of Orange II was measured by using a calibration plot. All experiments were repeated four times ( $n = 4$ ). The results showed that the developed sensor was most sensitive toward Orange II dye with % RSD in the range of 2.2–3.4% (Table 2). The percent

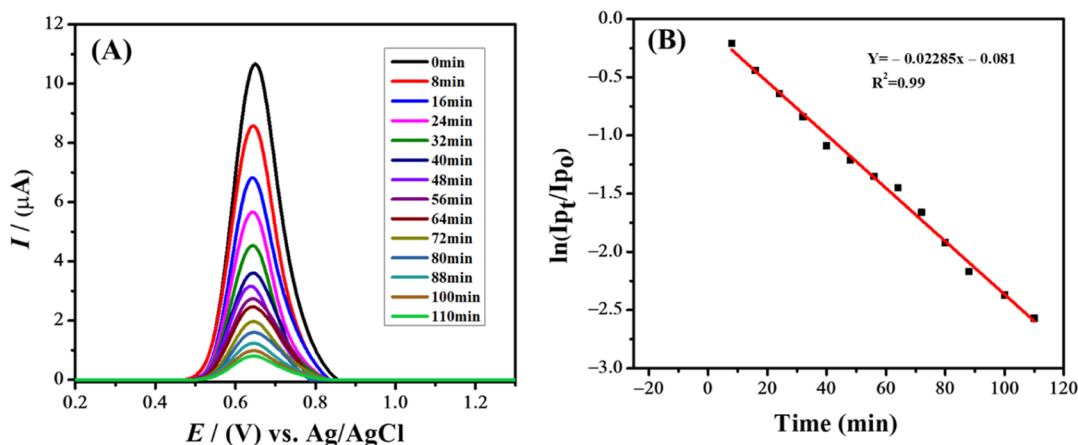


**Figure 7.** (A) SWVs of photodegradation of Orange II at different time intervals using  $\text{NH}_2\text{-fMWCNTs/ZnO/GCE}$  as a sensor. (B) Kinetic study of degradation using SWV data.

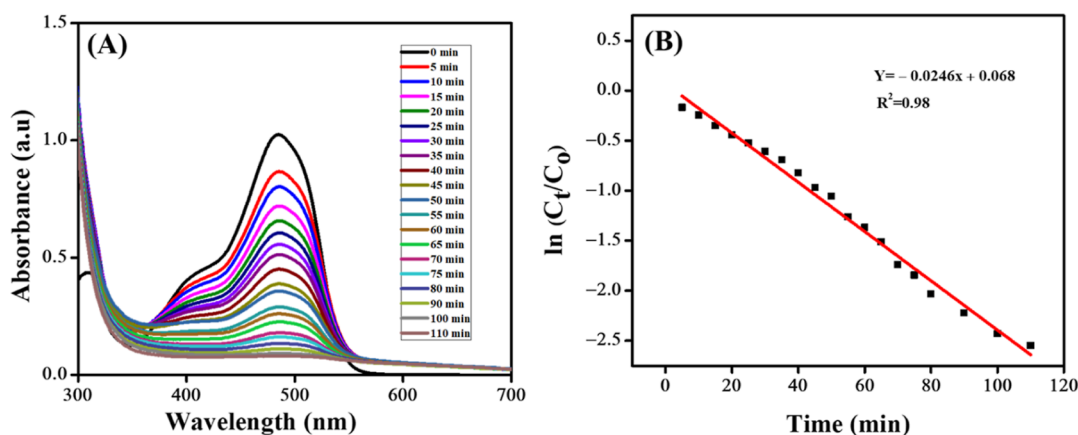


**Figure 8.** (A) UV-vis spectra of photodegradation of Orange II at different time intervals. (B) Photodegradation kinetics using UV-vis spectroscopic data.

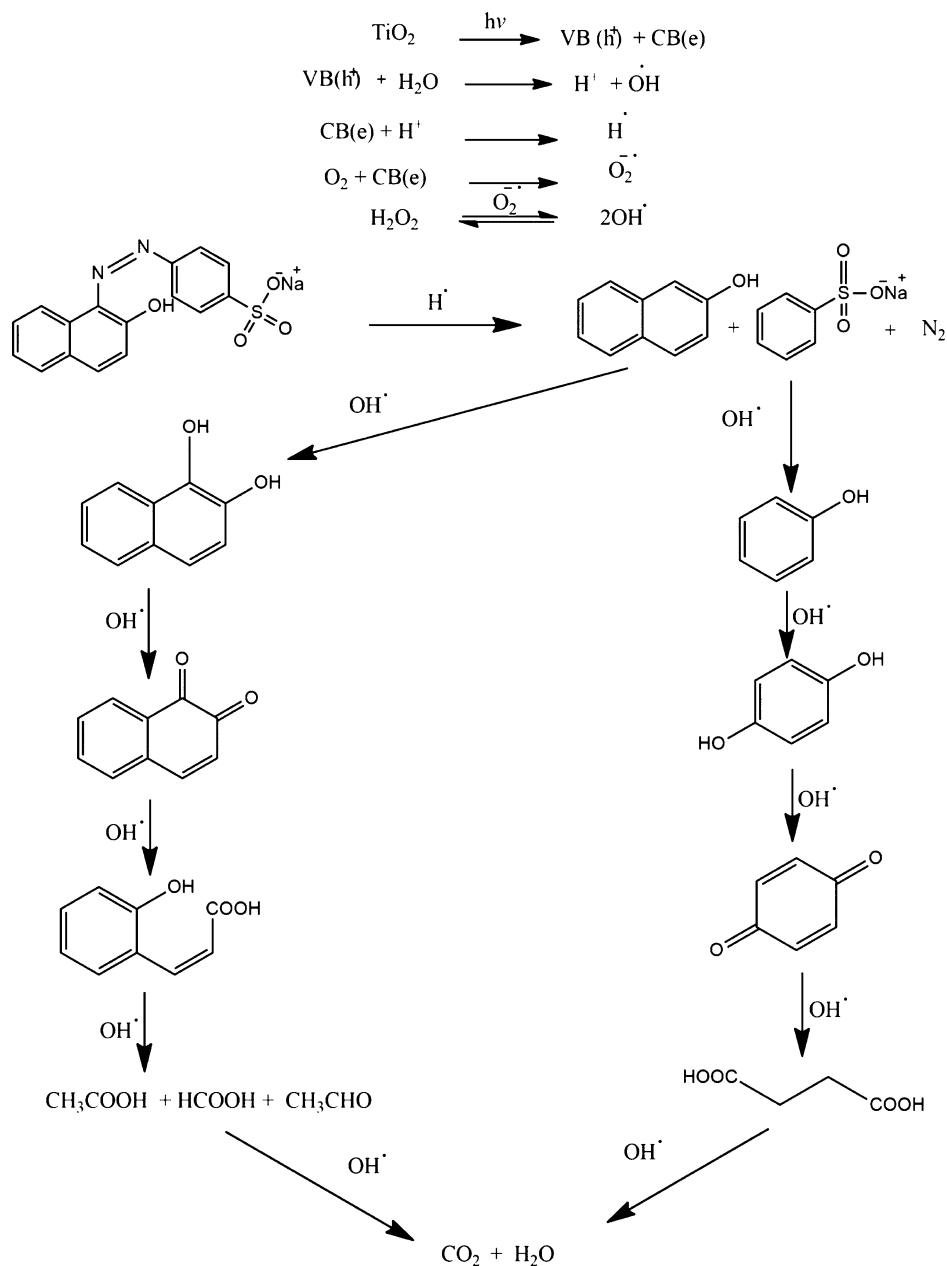
recoveries of the targeted analyte in the range of 96.00–98.33% suggest the real applicability of the designed sensor.

**3.10. Photodegradation Studies by the Designed Electrochemical Sensor.** Numerous ways have been developed and adopted for detoxifying dyes from the environment. Photodegradation is one of the most popular techniques. This is one of the most common methods for removing hazardous materials from the environment. Photodegradation of Orange II dye was carried out by using  $\text{TiO}_2$  as a photocatalyst and  $\text{H}_2\text{O}_2$  as an oxidizing agent. Using an electrochemical sensor, we observed and recorded the deterioration of the Orange II dye by SWV. The Orange II solution of the known concentration was kept in direct sunlight. The sample was obtained at various time intervals, and degradation was then investigated by recording the voltammogram. The voltammograms at various time intervals are depicted in Figure 7A. The concentration of dye in the sample diminishes with time, and the peak current corresponding to that period drops as well. Because the dye has entirely deteriorated in the presence of sunlight, the corresponding current has thus reached its lowest value. The impact of the irradiation period on Orange II photodegradation was also tested with the findings, as displayed in Figure S6A. The percentage degradation of the Orange II was obtained as 92% after 110 min. A kinetic investigation of Orange II photodegradation was also carried out, with the

residual concentration in the sample shown with time and the rate constant calculated. As shown in Figure 7B, the graph of  $\ln[(I_p)_t/(I_p)_0]$  as a function of time was constructed using a first-order rate equation to validate the order of the reaction. Using the formula  $\ln[(I_p)_t/(I_p)_0] = -kt$ , it was confirmed that the photodegradation process was best followed by a pseudo-first-order kinetics where  $(I_p)_0$  denotes the initial peak current at time  $t = 0$  and  $(I_p)_t$  denotes the peak current at time  $t$ . The resultant plot is a straight line, indicating it as a conventional first-order response plot.

**3.11. Photocatalytic Degradation Studies of Orange II Using an UV-Visible Spectrophotometer.** UV-vis spectroscopy was also used to examine the deterioration of Orange II dye. Figure 8A depicts the absorption spectra observed at different time intervals. Light absorption can cause the dye to degrade by generating electron-hole pairs in the catalyst  $\text{TiO}_2$ . The breakdown of organic molecules is mostly caused by the  $\cdot\text{OH}$  radicals, which have the second highest oxidation potential after fluorine. The effective electron trapping ability of oxygen helps stop the recombination of electrons with photogenerated holes. The efficiency of the photocatalytic processes is reduced when oxygen is limited due to the quick recombination of photogenerated electrons and holes in  $\text{TiO}_2$ , which limits the applicability of such a system in real-world applications. The addition of oxidants enhances the performance of  $\text{TiO}_2$  by eradicating the recombination process



Scheme 2. Mechanism of Orange II Dye Degradation by Sunlight in the Presence of TiO<sub>2</sub> and H<sub>2</sub>O<sub>2</sub>

as the added oxidants quickly interact with conduction band electrons to produce extremely reactive oxidizing radicals. The photodegradation efficiency is increased by using H<sub>2</sub>O<sub>2</sub> to prevent the recombination of electron/hole pairs. The proposed mechanism of dye degradation is shown in Scheme 2.

The oxidative degradation of Orange II is aided by H<sub>2</sub>O<sub>2</sub>. It may be explained as sunlight assisting in the mixing of photocatalyst nanoparticles with substrate dye molecules. The breakdown of the substrate molecules happens once the substrate encounters the photocatalyst nanoparticles. The impact of irradiation duration on UV–visible spectroscopic tests was also investigated, and the results are shown in Figure S6B. The highest decomposition of Orange II solution (92%) was recorded by an UV–visible spectrophotometer after 110 min. The spectroscopic percentage degradation is consistent with the electrochemical result. Spectroscopic data values were

also used to conduct a kinetic investigation of Orange II photodegradation. The reaction sequence was checked by displaying the graph of  $\ln(C_t/C_0)$  and time, as shown in Figure 8B. The rate constant ( $k$ ) of the reaction is calculated as  $\ln C_t/C_0 = -kt$ , where  $C_0$  is the maximal absorbance at time  $t = 0$  and  $C_t$  is the absorbance at time  $t$ . When a graph of  $\ln(C_t/C_0)$  and time is drawn, a straight line is obtained. This is an example of a first-order response plot. The rate constant is given by the slope value obtained from the linear plot. The disappearance of color by degradation is shown in Figure S7.

#### 4. CONCLUSIONS

A sensitive and stable sensor based on GCE modified with NH<sub>2</sub>-fMWCNTs and ZnO nanoparticles was developed for the nanomolar detection of Orange II dye. The components of the recognition layer significantly enhanced the peak current response of Orange II dye as compared to that of bare GCE.

The greater surface area and lower charge-transfer resistance of the modified electrode resulted in the intense oxidation signal of Orange II dye. Under optimized conditions, the LOD with a value of 0.57 nM was determined from the slope of the linear calibration plot. The dye was found to be oxidized in a pH-dependent manner involving proton-coupled electron-transfer oxidation. The sensor demonstrated the qualities of reproducibility and repeatability. The sensor also showed promise for monitoring the photocatalytic degradation of Orange II dye. The obtained results reveal the practical applicability of the designed sensing platform in real matrixes with high recoveries. The photocatalytic degradation of Orange II dye was assisted by TiO<sub>2</sub> nanoparticles, which act as a photocatalyst in the presence of H<sub>2</sub>O<sub>2</sub> which serves as an oxidizing agent. The percent degradation evaluated by employing voltammetric and spectrophotometric methods was found to be 92% in 110 min. The photocatalytic degradation studies suggest that combination of titania and hydrogen peroxide efficiently degrade the dye. The decolorization of Orange II dye in the presence of the photocatalyst offered visual evidence of dye degradation. The results of both electrochemical and UV-vis spectrophotometric techniques suggested that the breakdown of Orange II dye follows first-order kinetics. In future, the applicability horizon of such sensors may be extended by coupling them with industries for early sensing and degradation of pollutants prior to their release into freshwater bodies.

## ■ ASSOCIATED CONTENT


### SI Supporting Information

The Supporting Information is available free of charge at <https://pubs.acs.org/doi/10.1021/acsomega.2c03641>.

Calculated surface areas of bare and modified electrodes; EIS parameters: scan rate effect on anodic peak current of Orange II dye for determining adsorption or diffusion-controlled process at the NH<sub>2</sub>-f MWCNTs/ZnO/GCE; study of various supporting electrolytes on the anodic peak current of Orange II using NH<sub>2</sub>-fMWCNTs/ZnO/GCE; study of various optimization parameters on Orange II dye peak current, that is, deposition potential and deposition time; repeatability and reproducibility of the modified electrode; effect of irradiation time on Orange II degradation using voltammetric and spectroscopic techniques; and visual color variation of Orange II dye using TiO<sub>2</sub> nanoparticles and H<sub>2</sub>O<sub>2</sub> under direct sunlight (PDF)

## ■ AUTHOR INFORMATION


### Corresponding Authors

**Afzal Shah** – Department of Chemistry, Quaid-i-Azam University, Islamabad 45320, Pakistan;  [orcid.org/0000-0002-9465-9185](https://orcid.org/0000-0002-9465-9185); Email: [afzals\\_qau@yahoo.com](mailto:afzals_qau@yahoo.com)

**Iltaf Shah** – Department of Chemistry, College of Science, United Arab Emirates University, Al Ain 15551, United Arab Emirates; Email: [altafshah@uaeu.ac.ae](mailto:altafshah@uaeu.ac.ae)

### Authors

**Muhammad Irfan** – Department of Chemistry, Quaid-i-Azam University, Islamabad 45320, Pakistan

**Faiza Jan Iftikhar** – NUTECH School of Applied Science & Humanities, National University of Technology, Islamabad 44000, Pakistan;  [orcid.org/0000-0002-8669-3711](https://orcid.org/0000-0002-8669-3711)

**Mazhar Hayat** – Department of Chemistry, Quaid-i-Azam University, Islamabad 45320, Pakistan

**Muhammad Naeem Ashiq** – Institute of Chemical Sciences, Bahauddin Zakaria University, Multan 6100, Pakistan

Complete contact information is available at:

<https://pubs.acs.org/10.1021/acsomega.2c03641>

## ■ Author Contributions

Conceptualization, A.S. and M.I.; methodology, M.I., F.J.I., and M.H.; software, F.J.I.; validation, M.N.A., I.S., and A.S.; formal analysis, M.I. and M.H.; investigation, M.I.; resources, I.S., A.S., and M.N.A.; data curation, F.J.I.; writing—original draft preparation, M.I. and F.J.I.; writing—review and editing, A.S., I.S., and M.N.A.; visualization, M.I. and M.H.; and supervision, A.S.

## ■ Notes

The authors declare no competing financial interest.

## ■ ACKNOWLEDGMENTS

A.S. graciously acknowledges the generous support of Quaid-i-Azam University, Islamabad, Pakistan. I.S. graciously acknowledges the generous support of UAE University, UAE (12S091 UPAR).

## ■ REFERENCES

- (1) Pereira, J. C. Environmental issues and international relations, a new global (dis)order - the role of International Relations in promoting a concerted international system. *Rev. Bras. de Política Int.* **2015**, *58*, 191–209.
- (2) Khalid, S.; Shahid, M.; Natasha, I.; Bibi, T.; Sarwar, A. H.; Shah, N. K.; Niazi, N. A review of environmental contamination and health risk assessment of wastewater use for crop irrigation with a focus on low and high-income countries. *Int. J. Environ. Res. Public Health* **2018**, *15*, 895.
- (3) Hewlings, S. J.; Kalman, D. S. Curcumin: A review of its effects on human health. *Foods* **2017**, *6*, 92.
- (4) Nweke, O. C.; Sanders III, W. H., III Modern environmental health hazards: a public health issue of increasing significance in Africa. *Environ. Health Perspect.* **2009**, *117*, 863–870.
- (5) Dastoorpoor, M.; Sekhavatpour, Z.; Masoumi, K.; Mohammadi, M. J.; Aghababaeian, H.; Khanjani, N.; Hashemzadeh, B.; Vahedian, M. Air pollution and hospital admissions for cardiovascular diseases in Ahvaz, Iran. *Sci. Total Environ.* **2019**, *652*, 1318–1330.
- (6) Brillias, E.; Martínez-Huitle, C. A. Decontamination of wastewaters containing synthetic organic dyes by electrochemical methods. An updated review. *Appl. Catal., B* **2015**, *166–167*, 603–643.
- (7) Pimenta, L. P.; Gomes, D. C.; Cardoso, P. G.; Takahashi, J. A. Recent findings in azaphilone pigments. *J. Fungi* **2021**, *7*, 541.
- (8) Gan, T.; Sun, J.; Lin, Z.; Li, Y. Highly sensitive determination of Orange II based on the dual amplified electrochemical signal of graphene and mesoporous TiO<sub>2</sub>. *Anal. Methods* **2013**, *5*, 2964–2970.
- (9) Yadav, A.; Kumar, A.; Dwivedi, P. D.; Tripathi, A.; Das, M. In vitro studies on immunotoxic potential of Orange II in splenocytes. *Toxicol. Lett.* **2012**, *208*, 239–245.
- (10) Sun, Y.; Li, W.; Zhao, L.; Li, F.; Xie, Y.; Yao, W.; Liu, W.; Lin, Z. Simultaneous SERS detection of illegal food additives rhodamine B and basic Orange II based on Au nanorod-incorporated melamine foam. *Food Chem.* **2021**, *357*, 129741.
- (11) Garg, S. K.; Tripathi, M. Process parameters for decolorization and biodegradation of Orange II (Acid Orange 7) in dye-simulated minimal salt medium and subsequent textile effluent treatment by *Bacillus cereus* (MTCC 9777) RMLAU1. *Environ. Monit. Assess.* **2013**, *185*, 8909–8923.

- (12) Divya, N.; Bansal, A.; Jana, A. Photocatalytic degradation of azo dye Orange II in aqueous solutions using copper-impregnated titania. *Int. J. Environ. Sci. Technol.* **2013**, *10*, 1265–1274.
- (13) Ganguly, M.; Ariya, P. A. Novel technology for the removal of brilliant green from water: influence of post-oxidation, environmental conditions, and capping. *ACS Omega* **2019**, *4*, 12107–12120.
- (14) Gauthama, B. U.; Narayana, B.; Sarojini, B.; Bello, K.; Suresh, N. Nitrate/Nitrite determination in water and soil samples accompanied by in situ azo dye formation and its removal by superabsorbent cellulose hydrogel. *SN Appl. Sci.* **2020**, *2*, 1225.
- (15) David, I. G.; Buleandă, M.; Popa, D. E.; Bercea, A. M.; Ciucu, A. A. Simple Electrochemical Chloramphenicol Assay at a Disposable Pencil Graphite Electrode by Square Wave Voltammetry and Linear Sweep Voltammetry. *Anal. Lett.* **2021**, *55*, 1531–1548.
- (16) Yogeswaran, U.; Chen, S.-M. A review on the electrochemical sensors and biosensors composed of nanowires as sensing material. *Sens* **2008**, *8*, 290–313.
- (17) Zhu, L.; Zeng, W. Room-temperature gas sensing of ZnO-based gas sensor: A review. *Sens. Actuators, A* **2017**, *267*, 242–261.
- (18) Guo, D.-Y.; Shan, C.-X.; Qu, S.-N.; Shen, D.-Z. Highly sensitive ultraviolet photodetectors fabricated from ZnO quantum dots/carbon nanodots hybrid films. *Sci. Rep.* **2014**, *4*, 7469.
- (19) Kim, G. E.; Noh, S.; Kang, S. H.; Kim, Y. D.; Kim, T. K. Heat treatment effect on the behavior of oxide particles in mechanically alloyed oxide dispersion strengthened powders. *Sci. Adv. Mater.* **2017**, *9*, 2126–2130.
- (20) Hieu, N. M.; Kim, H.; Kim, C.; Hong, S.-K.; Kim, D. A hydrogen sulfide gas sensor based on pd-decorated ZnO nanorods. *J. Nanosci. Nanotechnol.* **2016**, *16*, 10351–10355.
- (21) Azizi-Lalabadi, M.; Hashemi, H.; Feng, J.; Jafari, S. M. Carbon nanomaterials against pathogens; the antimicrobial activity of carbon nanotubes, graphene/graphene oxide, fullerenes, and their nanocomposites. *Adv. Colloid Interface Sci.* **2020**, *284*, 102250.
- (22) Li, C.; Shi, G. Carbon nanotube-based fluorescence sensors. *J. Photochem. Photobiol., C* **2014**, *19*, 20–34.
- (23) Danish, M. S. S.; Estrella, L. L.; Alemaida, I. M. A.; Lysin, A.; Moiseev, N.; Ahmadi, M.; Nazari, M.; Wali, M.; Zaheeb, H.; Senjyu, T. Photocatalytic applications of metal oxides for sustainable environmental remediation. *Metals* **2021**, *11*, 80.
- (24) Yu, X.; Yin, H.; Ye, J. S.; Peng, H.; Lu, G.; Dang, Z. Degradation of tris-(2-chloroisopropyl) phosphate via UV/TiO<sub>2</sub> photocatalysis: Kinetic, pathway, and security risk assessment of degradation intermediates using proteomic analyses. *Chem. Eng. J.* **2019**, *374*, 263–273.
- (25) Shahhiraan, A. F.; Mahirah Ramli, R.; Mohd Zaid, H. F. Modified Titania Impact on Photocatalytic Efficiency of Bmim [Cl]. *J. Chem. Health Risks* **2021**, *11*, 283–290.
- (26) Wu, Z.; Guo, K.; Cao, S.; Yao, W.; Piao, L. Synergetic catalysis enhancement between H<sub>2</sub>O<sub>2</sub> and TiO<sub>2</sub> with single-electron-trapped oxygen vacancy. *Nano Res* **2020**, *13*, 551–556.
- (27) Cicvarić, K.; Meng, L.; Newbrook, D. W.; Huang, R.; Ye, S.; Zhang, W.; Hector, A. L.; Reid, G.; Bartlett, P. N.; de Groot, C. K. Thermoelectric properties of bismuth telluride thin films electro-deposited from a nonaqueous solution. *ACS Omega* **2020**, *5*, 14679–14688.
- (28) Shah, A. H.; Zaid, W.; Shah, A.; Rana, U. A.; Hussain, H.; Ashiq, M. N.; Qureshi, R.; Badshah, A.; Zia, M. A.; Kraatz, H.-B. pH Dependent electrochemical characterization, computational studies and evaluation of thermodynamic, kinetic and analytical parameters of two phenazines. *J. Electrochem. Soc.* **2014**, *162*, H115.
- (29) Babar, N.-U.-A.; Joya, K. S.; Tayyab, M. A.; Ashiq, M. N.; Sohail, M. Highly sensitive and selective detection of arsenic using electrogenerated nanotextured gold assemblage. *ACS Omega* **2019**, *4*, 13645–13657.
- (30) Li, J.; Feng, H.; Li, J.; Feng, Y.; Zhang, Y.; Jiang, J.; Qian, D. Fabrication of gold nanoparticles-decorated reduced graphene oxide as a high performance electrochemical sensing platform for the detection of toxicant Sudan I. *Electrochim. Acta* **2015**, *167*, 226–236.
- (31) Chattaraj, P. K.; Maiti, B. HSAB Principle Applied to the Time Evolution of Chemical Reactions. *J. Am. Chem. Soc.* **2003**, *125*, 2705–2710.
- (32) Zhang, X.; Shen, Y.; Shen, G.; Zhang, C. Simple and Effective Approach to Prepare an Epoxy-Functionalized Polymer and Its Application for an Electrochemical Immunosensor. *ACS Omega* **2021**, *6*, 3637–3643.
- (33) Garimella, L. B.; Dhiman, T. K.; Kumar, R.; Singh, A. K.; Solanki, P. R. One-step synthesized ZnO np-based optical sensors for detection of aldicarb via a photoinduced electron transfer route. *ACS Omega* **2020**, *5*, 2552–2560.
- (34) Shah, A.; Malik, M. S.; Zahid, A.; Iftikhar, F. J.; Anwar, A.; Akhter, M. S.; Shah, M. R.; Zia, M. A.; Ashiq, M. N.; Shah, A. H. Carbamazepine coated silver nanoparticles for the simultaneous electrochemical sensing of specific food toxins. *Electrochimica Acta* **2018**, *274*, 131–142.
- (35) Gowda, J. I.; Nandibewoor, S. T. Electrochemical behavior of paclitaxel and its determination at glassy carbon electrode. *Asian J. Pharm. Sci.* **2014**, *9*, 42–49.
- (36) Wang, J.; Yang, B.; Wang, H.; Yang, P.; Du, Y. Highly sensitive electrochemical determination of Sunset Yellow based on gold nanoparticles/graphene electrode. *Anal. Chim. Acta* **2015**, *893*, 41–48.
- (37) Kokab, T.; Shah, A.; Iftikhar, F. J.; Nisar, J.; Akhter, M. S.; Khan, S. B. Amino Acid-Fabricated Glassy Carbon Electrode for Efficient Simultaneous Sensing of Zinc(II), Cadmium(II), Copper(II), and Mercury(II) Ions. *ACS Omega* **2019**, *4*, 22057–22068.
- (38) Shah, A.; Malik, M. S.; Zahid, A.; Iftikhar, F. J.; Anwar, A.; Akhter, M. S.; Shah, M. R.; Zia, M. A.; Ashiq, M. N.; Shah, A. H. Carbamazepine coated silver nanoparticles for the simultaneous electrochemical sensing of specific food toxins. *Electrochim. Acta* **2018**, *274*, 131–142.
- (39) Gao, Y.; Xie, Z.; Zhang, Y.; Zou, L.; Ye, B. A simple and sensitive voltammetric method for the determination of Orange II based on a functionalized graphene-modified electrode. *J. AOAC Int.* **2016**, *99*, 1287–1294.
- (40) Liu, Z.; Zhai, H.; Chen, Z.; Zhou, Q.; Liang, Z.; Su, Z. Simultaneous determination of Orange G and Orange II in industrial wastewater by a novel Fe<sub>2</sub>O<sub>3</sub>/MWCNTs-COOH/OP modified carbon paste electrode. *Electrochim. Acta* **2014**, *136*, 370–376.
- (41) Wu, L.; Pu, H.; Huang, L.; Sun, D.-W. J. F. C. Plasmonic nanoparticles on metal-organic framework: A versatile SERS platform for adsorptive detection of new coccine and Orange II dyes in food. *Food Chem.* **2020**, *328*, 127105.
- (42) Wang, Q.; Shi, Z.; Wang, Z.; Zhao, Y.; Li, J.; Hu, H.; Bai, Y.; Xu, Z.; Zhangsun, H.; Wang, L. Rapid simultaneous adsorption and SERS detection of acid Orange II using versatile gold nanoparticles decorated NH<sub>2</sub>-MIL-101(Cr). *Anal. Chim. Acta* **2020**, *1129*, 126–135.